Mechanism of Ligand Substitution on High-Spin Iron(III) by Hydroxamic Acid Chelators. Thermodynamic and Kinetic Studies on the Formation and Dissociation of a Series of Monohydroxamatoiron(III) Complexes

Bruce Monzyk and Alvin L. Crumbliss*

Contribution from the Department of Chemistry, P. M. Gross Chemistry Laboratory, Duke University, Durham, North Carolina 27706. *Received March 1, 1979*

Abstract: Thermodynamic and kinetic studies were performed to investigate the complexation of aqueous high-spin iron(III) by six bidentate hydroxamic acids, $R_1C(O)N(OH)R_2$ ($R_1 = CH_3$ or C_6H_5 and R_2 = H, CH_3, or C_6H_5) in acid medium. Both complex formation and dissociation (aquation) reactions were investigated over the temperature and $[H^+]$ ranges of 2–50 °C and 0.025–1.1 M, respectively. Complexation occurs by coordination of both oxygen atoms of the ligand to the iron(III) center, with concomitant loss of a proton yielding 1:1 complexes of the type $[Fe(R_1C(O)N(O)R_2)(H_2O)_4]^{2+}$. The thermodynamic driving force for complex formation (Q_f for path 1) is an increase in entropy, with the enthalpy of formation actually opposing complex formation. The $\Delta S_f°$ values are essentially constant and $\Delta H_f°$ values correlate with the variations in overall thermodynamic stability. Complex stability was found to parallel systematic variations in the electron donor or acceptor ability of the R_1 and R_2 substituents (as defined by σ^+) with R_2 showing the major effect. Kinetic studies were performed in two ways: as a second-order complex formation process going to equilibrium ($k_{exp}^{form} = k_a' + k_b'/[H^+]$) and as a relaxation process ($k_{exp}^{ret} = k_a + k_b/[H^+] + k_c[H^+]$) caused by rapidly increasing the $[H^+]$. Both methods gave equivalent results which were interpreted on the basis of a parallel path mechanism involving substitution on $Fe(H_2O)_6^{3+}$ and $Fe(H_2O)_5OH^{2+}$ by the undissociated hydroxamic acid (HA): $Fe(H_2O)_6^{3+} + HA \rightleftharpoons Fe(A)(H_2O)_4^{2+} + H^+$ (k_1, k_{-1}) (path 1); $Fe(H_2O)_5OH^{2+} + HA \rightleftharpoons Fe(A)(H_2O)_4^{2+}$ (k_2, k_{-2}) (path 2). The reaction path involving $Fe(H_2O)_6^{3+}$ and A^-_{aq} can be excluded based on experimental evidence. Most of the reaction occurs via path 2 over the $[H^+]$ range investigated. The magnitudes of the rate constants indicate that ring closure is not rate determining in either path. Activation parameters for complex formation via both paths show competing effects in $\Delta H^{\ddagger}$ and $\Delta S^{\ddagger}$ (isokinetic relationship) which is reflected in only small variations in the observed formation rate constants. Isokinetic behavior is also exhibited by both complex dissociation paths. The variations in complex aquation rates at 25 °C via path 2 (which is independent of $[H^+]$) are controlled by variations in $\Delta S^{\ddagger}_{-2}$. These variations in $\Delta S^{\ddagger}_{-2}$ show the same trends with changes in R_1 and R_2 as that found for the overall thermodynamic stability (Q_f) of the complexes. In contrast, variations in aquation rates via path 1 at 25 °C are controlled by variations in $\Delta H^{\ddagger}_{-1}$, which correlate with ligand acid strength(pK_a). These results for complex aquation are interpreted on the basis of a two-path mechanism involving a common intermediate (singly bonded ligand) which can undergo further spontaneous bond cleavage (path 2), or acquire a H^+_{aq} (depending upon $[H^+]$ and ligand basicity) and then aquate (path 1). In both paths, variations in thermodynamic stability are reflected in the variations in the aquation rates. The major influence of R_2 is attributed to its direct influence in stabilizing positive charge density on nitrogen which thereby enhances the degree of delocalization of the lone pair of electrons on nitrogen into the carbonyl function. LFERs suggest that this in turn stabilizes the ground state ($\Delta H_f°$) and destabilizes the transition state ($\Delta S^{\ddagger}_{-2}$). Hence, the aquation studies indicate the presence of some degree of associative character during complex formation. Although the rate constants for complex formation via either path do not vary widely, the associated activation parameters do and are also consistent with some associative character in complex formation with $Fe(H_2O)_5OH^{2+}$ as well as with $Fe(H_2O)_6^{3+}$. It is also concluded that stabilization of positive charge density on nitrogen in *any* way increases the acidity of the free ligand, while *only* stabilization of the resonance form corresponding to nitrogen lone pair delocalization into the carbonyl function stabilizes the monohydroxamatoiron(III) complex—both thermodynamically and kinetically.

Introduction

Hydroxamic acids are weak organic acids[1] with a wide variety of applications including use as commercial flotation reagents in extractive metallurgy, inhibitors for copper corrosion, antifungal agents, pharmaceuticals, food additives, and in nuclear fuel processing. One of the characteristics of hydroxamic acids is their ability to form stable transition metal complexes,[2] which forms the basis for their usefulness as analytical reagents.[3] The deep purple or red color of hydroxamatoiron(III) complexes serves as a fairly specific qualitative test for hydroxamic acids.

Some naturally occurring hydroxamic acids serve as iron(III) specific chelators. These compounds are called siderophores and are involved in microbial iron transport. Their specific function is to solubilize iron from the environment and transport it to the cell.[4-8] The specificity of hydroxamate siderophores for chelating iron(III) among the physiologically important metal ions, and their high complex formation constants, has led to investigations of their use as therapeutic agents for the treatment of iron overload in humans caused by β-thalassemia major. Deferriferrioxamine B is currently used for this purpose[9,10] and rhodotorulic acid has undergone preliminary clinical trials.[11] In addition to siderophores with hydroxamate structures, synthetic mono- and dihydroxamic acids have been tested for their efficacy in removing excess iron from hypertransfused mice.[12,13] At the other extreme of iron imbalance, tris(acetohydroxamato)iron(III) has been used to treat iron deficiency in anemic rats.[14]

Several X-ray structural reports of iron(III) complexes with synthetic[15] and naturally occurring[16-19] hydroxamic acids are available which show that the hydroxamate ion binds to iron(III) to form a five-membered chelate ring. Throughout this report the shorthand notation shown in I will be used, where

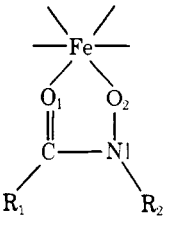

I

R_1, O_1 and R_2, O_2 represent the organic substituent and oxygen atom bonded to the C and N atoms, respectively.

0002-7863/79/1501-6203$01.00/0

Hydroxamatoiron(III) complexes characteristically have very high formation constants ($\log \beta_3 \sim 30$[20]). Although it has often been stated in the literature that hydroxamic acids (synthetic and natural) exhibit an unusual selectivity for high-spin iron(III), the available data[20] indicate that hydroxamic acids have a high affinity for spherically symmetric 3+ ions in general. The variations in thermodynamic stability among these complexes can readily be rationalized on the basis of the charge to radius ratio of the metal ion alone. Therefore, a more correct statement would be that hydroxamic acids exhibit a high specificity for iron(III) over other *biologically* important metal ions, since these other ions are mainly in the 2+ oxidation state. However, hydroxamate complexes of spherically symmetric 3+ metal ions do show a significant enhancement in thermodynamic stability over that for the typical carboxylate and aminocarboxylate ligands of equal denticity.[20] Therefore, it is of interest to determine which feature(s) of the hydroxamate functional group cause this observed enhanced thermodynamic stability. Of particular interest are the high-spin ferric systems, since these are related to the biologically important iron(III) chelating agents or siderophores.

Despite an active interest in the determination of stability constants for hydroxamate complexes of iron(III) from a number of laboratories,[3a,20-24] there are no temperature-dependence studies and very little kinetic data available. Iron(III) complex formation rate constants for deferriferrioxamine B[25] and four synthetic monohydroxamic acids[26] have been obtained, and kinetic data for removal of iron(III) from tris(acetohydroxamato)iron(III) by transferrin has been reported.[14] No aquation rate data are available for hydroxamatoiron(III) complexes, and in fact there is a scarcity of kinetic data available for iron(III) complex aquation reactions with a series of related ligands of any type.[27,28] Hydroxamic acids are excellent ligands for use in probing the mechanism of ligand substitution at an iron(III) center. Their iron(III) complexes are stable with respect to low pH, air oxidation, room light, and internal oxidation-reduction. The ligands themselves may be readily synthesized and afford a wide range of independent steric and electronic effects.

To aid in developing a better understanding of the enhanced thermodynamic stability of hydroxamatoiron(III) complexes and of the mechanism of substitution processes on high-spin iron(III) in general, we wish to report here on the complex formation constants, kinetics of formation and aquation, and associated temperature dependencies for a series of six related monohydroxamatoiron(III) complexes where $R_1 = CH_3$ or C_6H_5 and $R_2 = H$, CH_3, or C_6H_5.[29]

Experimental Section

Materials. Iron(III) perchlorate (G. F. Smith) was recrystallized twice from dilute perchloric acid before use. Sodium perchlorate was prepared by neutralization of Na_2CO_3 (Fisher, ACS certified) by $HClO_4$ (Fisher, ACS reagent), and was recrystallized from water prior to use. Potassium dichromate (MCB, ACS reagent) was recrystallized from water prior to use. All solutions were prepared using water which was purified by distilling conductivity water from acidic $K_2Cr_2O_7$, and then slowly from basic $KMnO_4$ in an all-glass apparatus with Teflon sleeves and stopcocks. $CH_3C(O)N(OH)H$, $C_6H_5C(O)N(OH)H$, and $C_6H_5C(O)N(OH)C_6H_5$ were purchased from Eastman Chemical Co., recrystallized twice from ethyl acetate, and dried in vacuo. $C_6H_5C(O)N(OH)CH_3$, $CH_3C(O)N(OH)CH_3$, and $CH_3C(O)N(OH)C_6H_5$ were prepared as described in the literature.[30-32] The purity of these compounds was checked by elemental (C, H, N) analysis (M-H-W Laboratories, Phoenix, Ariz.), melting point, ^1H NMR and IR spectra, and equivalent weights obtained from pH titrations.

Methods, Preparation of Solutions. Care was taken in the preparation and manipulation of iron(III) solutions in order to prevent extensive hydrolysis which would otherwise be expected to complicate equilibrium and kinetic measurements.[33] We have used the results of previous comprehensive studies to determine the extent and influence of iron(III) hydrolysis at various acidities, iron(III) concentrations, temperatures, and ionic strengths.[34-36] All of our studies were performed at conditions such that the only aqueous iron(III) species present to a significant extent were $Fe(H_2O)_6^{3+}$ and $Fe(H_2O)_5OH^{2+}$ and the maximum concentration of the latter was never more than 2% of the total amount of iron(III). Stock aqueous iron(III) solutions were prepared with [Fe(III)] ~ 0.1 M and [$HClO_4$] ~ 0.1 M.[37] The stock iron(III) solutions were standardized by titration with a standard solution of triply recrystallized $K_2Cr_2O_7$ after reduction with stannous ion according to established procedures.[38] The acidity of the stock iron(III) solutions ([$HClO_4$] ~ 0.1 M) was determined by passing an aliquot through a Dowex 50W-X8 20–50 mesh cation exchange resin in the acid form. The liberated H^+_{aq} ion was titrated with standardized NaOH to the phenolphthalein end point and corrections were made for the iron(III) present. All determinations were made in triplicate.

Reagent iron(III) solutions were prepared by dilution of the stock solution with aqueous $HClO_4/NaClO_4$ (adding the acid first) so that [Fe(III)] < 10^{-3} M, [$HClO_4$] = 0.03–0.8 M and [$NaClO_4$] such that the total ionic strength was 0.8 M. After dilution, at least 2 h is needed, and 3 h was allowed, for these solutions to reach equilibrium (relative to any hydrolysis products which were present in the more concentrated stock solution).

Stock $NaClO_4$ solutions, used to maintain constant ionic strength, were standardized by passing an aliquot through a Dowex 50W-X8 20–50 mesh cation exchange column in the acid form and titrating the liberated H^+ to the phenolphthalein end point.

Reagent hydroxamic acid (HA) ligand solutions ([HA] < 10^{-3} M, [$HClO_4$] = 0.03–0.8 M, I = 0.8 M ($NaClO_4$)) were used immediately after preparation. Kinetic experiments using a particular solution were completed in less than 3 h. At these conditions ligand hydrolysis was negligible.

Reagent monohydroxamatoiron(III) complex solutions (< 10^{-3} M) were carefully prepared (by weight) to contain equimolar amounts of iron(III) and ligand (±0.2%) at pH 2 (adding the acid first). After initial equilibration (~3 h) these solutions were used immediately, with a series of kinetic runs never lasting longer than 24 h. Separate spectral studies indicated these solutions to be stable at room temperature up to 4 days at pH 2. Solutions 1 day old and exposed to varying degrees of fluorescent room light showed the same spectral and kinetic behavior as fresh solutions. Complex solutions maintained at 50 °C for 15 h showed the same kinetic behavior as solutions stored for the same time at room temperature. When necessary, reagent solutions were stored overnight in a refrigerator.

The absorption maxima, λ_{max}, and molar absorptivities, ϵ, for the monohydroxamatoiron(III) complexes were determined from mole-ratio experiments at the conditions of excess iron(III) ([Fe(III)]/[HA] from 30 to 120), 0.1 M $HClO_4$, and 2.0 M ionic strength ($NaClO_4$). The λ_{max} and ϵ values for each of the complexes under investigation are listed below. The molar absorptivities and associated uncertainties were calculated from three to seven absorbance readings obtained using a Beckman Acta III recording double beam spectrophotometer equipped with a jacketed cell holder maintained at 25.0 °C: $[Fe(CH_3C(O)N(O)H)(H_2O)_4]^{2+}$, 500 nm, 871 (7) M^{-1} cm^{-1}; $[Fe(C_6H_5C(O)N(O)H)(H_2O)_4]^{2+}$, 515 nm, 1296 (15) M^{-1} cm^{-1}; $[Fe(CH_3C(O)N(O)C_6H_5)(H_2O)_4]^{2+}$, 505 nm, 1192 (10) M^{-1} cm^{-1}; $[Fe(C_6H_5C(O)N(O)C_6H_5)(H_2O)_4]^{2+}$, 515 nm, 1301 (8) M^{-1} cm^{-1}; $[Fe(CH_3C(O)N(O)CH_3)(H_2O)_4]^{2+}$, 510 nm, 1066 (7) M^{-1} cm^{-1}; $[Fe(C_6H_5C(O)N(O)CH_3)(H_2O)_4]^{2+}$, 508 nm, 696 (11) M^{-1} cm^{-1}.

Equilibrium Measurements. The determination of hydroxamic acid ligand pK_a values as a function of temperature is described elsewhere.[32] Data for monohydroxamatoiron(III) complex formation quotient calculations were obtained in two ways. In one method static measurements were made at 25.0 °C at a fixed [H^+] (0.1 M) and a variable [Fe(III)]/[HA] ratio (0.3–120) which corresponds to between 10 and 100% complex formation. These measurements were made in the region from 350 to 800 nm for each complex using a Beckman Acta III spectrophotometer equipped with a water-jacketed cell holder. For the other method, infinite time absorbance readings were taken from kinetic experiments where the [Fe(III)]/[HA] ratio was fixed ([Fe(III)] = [HA] = 10^{-3} M) and the [H^+] varied over the range from 0.025 to 1.05 M. In these determinations the stopped-flow spectrophotometer absorbance readings were checked against the Beckman Acta III recording double beam spectrophotometer. These data were collected over the temperature range from 0 to 50 °C and

were used to compute $\Delta H_f°$ and $\Delta S_f°$ values for complex formation.

Kinetic Measurements. An Aminco stopped-flow apparatus, employing a Beckman DU monochromator, was used for all of the kinetic measurements. Two methods of data collection were used. In earlier experiments oscilloscope tracings of photomultiplier output voltage as a function of time were recorded on Polaroid film. Reproducibility was checked by flowing the reactants together several times using the same time base and visually determining if the oscilloscope tracings were exactly superimposed. Once this condition was satisfied, three to five sets of data were collected at different sweep times. This process yielded from 20 to 55 data points per each observed rate constant. Voltage–time data were measured from the Polaroid photographs and the data analyzed using a Texas Instruments SR-52 programmable calculator and a DEC Model PDP 8/f computer. Later experiments utilized a digital data acquisition system developed by interfacing the Aminco instrument to a Cybertech LP-12 12-bit microcomputer. Data were collected on paper tape which was then read by a DEC Model PDP 8/f minicomputer for data analysis. As in the experiments using Polaroid film, data were collected only when the oscilloscope tracings were exactly superimposable. This process yielded from 40 to 55 data points per each observed rate constant. Several experiments were run using both data acquisition systems to ensure that there were no hidden artifacts associated with the method of data acquisition. Kinetic data were collected at the λ_{max} value for each of the monohydroxamatoiron(III) complexes.

Temperature control was maintained with the use of a Forma Scientific Model 2095 constant-temperature bath over a range of approximately 0–55 °C. Temperature control precision was ±0.05 °C over most of this range. The temperatures at which kinetic experiments were performed were obtained by measuring the temperature of the circulating liquid immediately after it exited from the syringe block of the stopped-flow apparatus. The reported temperatures are an average of 6–12 readings taken throughout a given experiment at a particular temperature. The maximum temperature difference between the bath and the spectrophotometer was +2 °C at 50 °C and −2 °C at 0 °C.

Formation kinetics were studied by flowing together an acidic reagent iron(III) solution (typically [Fe(III)] < 10^{-3} M, [$HClO_4$] = 0.03–0.8 M, I = 0.8 M ($NaClO_4/HClO_4$)) with an acidic solution of the ligand (typically [HA] < 10^{-3} M, [$HClO_4$] = 0.03–0.8 M, I = 0.8 M ($NaClO_4$)). Relaxation kinetics were studied by flowing together a monohydroxamatoiron(III) complex solution (typically [Fe(III)] = [HA] < 10^{-3} M, [$HClO_4$] = 0.01 M, I = 2.0 M ($NaClO_4/HClO_4$)), with a solution of increased acid concentration (typically [$HClO_4$] = 0.05–2.1 M, I = 2.0 M ($NaClO_4/HClO_4$)). Each experimental rate constant reported in the Results section represents 30–60 (normally 50) data points from 3 to 6 (normally 6) separate stopped-flow injections.

Results

Complex Stoichiometry. Spectral data collected over the wavelength range from 420 to 800 nm show a single λ_{max} and ϵ_{max} for the [Fe(III)]/[HA] ratios studied up to 120:1.[37] The shape and position of this absorption band remain constant and its absorptivity reaches a maximum at [Fe(III)]/[HA] ≃ 20:1, for [H^+] = 0.1 M and 25 °C. Spectral changes in the 350–420-nm region can be included in this analysis once allowance for the hydrolysis of the excess iron(III) present is made. A representative plot for the *N*-methylacetohydroxamic acid system is shown in Figure 1.

We have used matrix methods[39] to analyze spectral data for the number of absorbing species over the wavelength region from 350 to 800 nm at [Fe(III)]/[HA] ratios from 0.03 to 120 and [H^+] from 0.01 to 1.0 M. These data establish that only one absorbing species exists at our conditions for all of the six hydroxamic acid–iron(III) systems investigated. Therefore, if one makes the reasonable assumption that when [Fe(III)]/[HA] = 120 only the 1:1 complex, FeA^{2+}, is present, then the single absorbing species over the entire [Fe(III)]/[HA] and [H^+] range investigated must be FeA^{2+}. This assignment was verified by assuming the formation of FeA^{2+}, and then calculating ϵ_{app} for various [Fe(III)]/[HA] values for comparison with the observed absorbance. The excellent

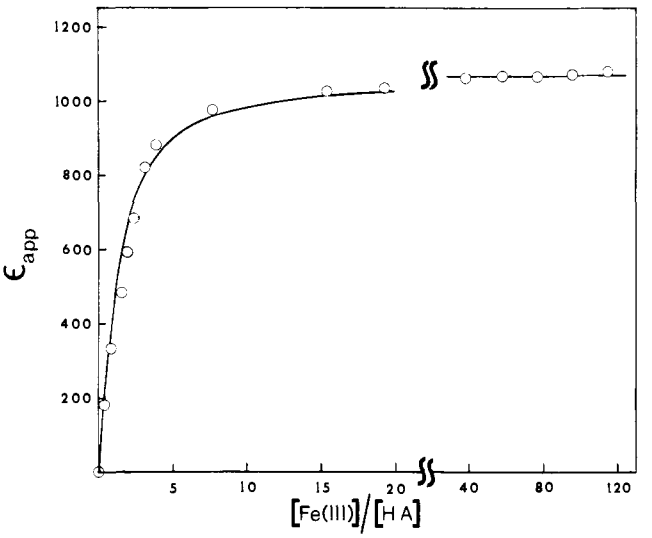

Figure 1. Apparent molar absorptivity (=Abs_e/C_{tot} where Abs_e = equilibrium absorbance and C_{tot} = total concentration of HA) plotted as a function of [Fe(III)]/[HA] ratio for the case where HA = $CH_3C(O)N(OH)CH_3$. Conditions: λ 510 nm; 25.0 (0.1) °C; [H^+] = 0.10 M; *I* = 1.10 M ($HClO_4/NaClO_4$); [HA] = 2.934×10^{-4} M. ϵ for FeA^{2+} calculated from data in the region where [Fe(III)]/[HA] > 20 is 1066 (7) cm^{-1} M^{-1}. Q_f for FeA^{2+} calculated from absorbance data in the region from 15 to 85% of the maximum absorbance is 316 (39). Solid line computed assuming 1:1 complex stoichiometry using an average Q_f value obtained from all data where [Fe(III)]/[HA] < 20.

agreement between calculated and observed values shown in Figure 1 for the *N*-methylacetohydroxamic acid–iron(III) system is representative of that found for all six hydroxamic acids investigated and indicates that at our conditions only a 1:1 complex is formed. As required, similar calculations assuming a 1:2 or 2:1 complex as the sole absorbing species provided poor agreement between calculated ϵ_{app} and the observed absorbance in all cases. In addition, consistent with this assignment the data for all six hydroxamic acid systems yield linear plots of a rearranged form of the equilibrium expression (see eq 3 below) corresponding to the formation of a 1:1 complex. Literature data for aceto- and benzohydroxamic acid also suggest that the monohydroxamatoiron(III) complexes should be the only complexes formed at our conditions.[21]

Additional characterization of the iron(III) complex formed in the case of *N*-methylbenzohydroxamic acid was obtained by the method of continuous variations.[40] The absorbance vs. mole fraction plots exhibited a maximum at 0.5 (±2%) mole fraction, indicating that the absorbing species contains hydroxamic acid and iron(III) in a 1:1 ratio.

Equilibrium Studies. Acid dissociation constants, pK_a, and the associated temperature dependencies were determined for all six hydroxamic acids as described elsewhere[32] using conditions identical with the complexation studies. These results are shown in Table I. While the pK_a values vary systematically with the R_1 and R_2 substituents, they fall in the approximate range from 8 to 9, and the hydroxamic acids are therefore undissociated at the conditions of our complexation studies. The reaction of interest in our investigation is the formation of the monohydroxamatoiron(III) complex from hexaaquoiron(III) and free hydroxamic acid ligand:

$$Fe(H_2O)_6^{3+} + R_1C(O)N(OH)R_2 \overset{H_2O}{\rightleftharpoons} Fe(R_1C(O)N(O)R_2)(H_2O)_4^{2+} + H^+_{aq} + 2H_2O \quad (1)$$

Since this investigation was carried out at conditions such that the bis and tris complexes were not formed and hence $[Fe(R_1C(O)N(O)R_2)(H_2O)_4]^{2+}$ was the only absorbing

Table I. Thermodynamic Data for Monohydroxamatoiron(III) Complex Formation

$R_1C(O)N(OH)R_2$ R_1	R_2	pK_a[a]	Q_f[b]	$\Delta H_f°$,[c] kcal/mol	$\Delta S_f°$,[c] eu	$10^{-10}\,Q_f'$,[d] M^{-1}	$\Delta H_f°'$,[e] kcal/mol	$\Delta S_f°'$,[e] eu
CH_3	H	9.02(0.02)	109(6)	2.3(0.2)	16(1)	8.57	−2.1(0.8)	43(3)
C_6H_5	H	8.50(0.01)	172(7)	2.6(0.1)	18.8(0.2)	4.78	−2.9(0.4)	39(1)
CH_3	C_6H_5	8.34(0.02)	225(9)	1.3(0.1)	15.6(0.4)	6.01	−9.1(1.1)	19(4)
C_6H_5	C_6H_5	7.98(0.01)	266(25)	1.1(0.1)	14.7(0.1)	2.55	−6.5(0.2)	26(1)
CH_3	CH_3	8.65(0.3)	316(39)	0.6(0.1)	14.6(0.5)	23.3	−0.5(0.5)	50(2)
C_6H_5	CH_3	7.87(0.05)	549(22)	1.0(0.2)	16.7(0.8)	6.28	−2.9(0.9)	40(3)

[a] From ref 32. [b] Formation quotient for reaction 1 calculated according to eq 2. Values listed represent an average of seven to ten determinations at different [Fe(III)]/[HA] ratios. Q_f values were found to be independent of λ (350–800 nm). For greater precision reported constants were calculated from data obtained at λ_{max}. T = 25.0 °C, I = 1.10 M ($NaClO_4/HClO_4$). [c] $\Delta H_f°$ and $\Delta S_f°$ for reaction 1 calculated from Q_f data obtained from eq 3 over the following temperature ranges (R_1, R_2, T_{range}): CH_3, H, 2.5–51.3 °C; C_6H_5, H, 2.0–50.4 °C; CH_3, C_6H_5, 25.0–51.3 °C; C_6H_5, C_6H_5, 15.3–50.3 °C; CH_3, CH_3, 14.8–49.3 °C; C_6H_5, CH_3, 13.8–45.7 °C. Values listed represent an average of 15–20 determinations at each of 3–6 (normally 4) temperatures. I = 2.00 M ($NaClO_4/HClO_4$). [d] Formation quotient for non-experimentally-accessible reaction 8 calculated according to $Q_f' = Q_f/K_a$ at 25 °C; see text. [e] $\Delta H_f°'$ and $\Delta S_f°'$ for non-experimentally-accessible reaction 8 calculated from $\Delta H_f°$, $\Delta S_f°$ for reaction 1. $\Delta H_a°$, $\Delta S_a°$ for reaction 7 obtained from ref 32.

species in solution, the equilibrium quotient, Q_f, for reaction 1 was calculated in the usual way from the equation

$$Q_f = \frac{[FeA^{2+}][H^+]}{[Fe^{3+}][HA]} \tag{2}$$

(For clarity, HA and A^- represent the hydroxamic acid and hydroxamate anion, respectively, and coordinated H_2O is omitted.) The various quantities in eq 2 were determined as follows: $[FeA^{2+}] = Abs/\epsilon$ at the λ_{max} value for each complex; $[Fe^{3+}] = [Fe(III)]_{tot} - [FeA^{2+}]$; $[HA] = [HA]_{tot} - [FeA^{2+}]$. $[H^+]$ was in large excess and was calculated from the known acidities of the reagents.

Equilibrium quotients, Q_f, for reaction 1 were calculated from data such as is shown in Figure 1 using the [Fe(III)]/[HA] ratios where complex formation was between 15 and 85% complete, and eq 2. The results of these experiments performed at 25.0 °C are listed in Table I. Values obtained for acetohydroxamic acid and benzohydroxamic acid show good agreement with literature values when corrections are made for differing conditions.[21]

Enthalpy ($\Delta H_f°$) and entropy ($\Delta S_f°$) changes associated with complex formation were calculated from equilibrium $[FeA^{2+}]$ concentrations determined over a 40 °C temperature range. These data were obtained from kinetic experiments (described below and in the Experimental Section). The experimental conditions allowed Q_f to be calculated at each temperature according to the equation

$$\frac{C_{tot}}{Abs_e} = \frac{([H^+]/Abs_e)^{1/2}}{(\epsilon Q_f)^{1/2}} + 1/\epsilon \tag{3}$$

where $C_{tot} = [Fe(III)]_{tot} = [HA]_{tot}$ and Abs_e = total absorbance at equilibrium, Q_f was obtained from the slope of a plot of C_{tot}/Abs_e vs. $([H^+]/Abs_e)^{1/2}$, using a value for ϵ obtained from mole-ratio plots described above.[41] These results, in the form of $\Delta H_f°$ and $\Delta S_f°$ values for reaction 1, are listed in Table I.

The Q_f values obtained in this study show a systematic trend when R_1 and R_2 are varied. Increasing Q_f values follow the order R_2 = H < C_6H_5 < CH_3 (primary effect) and R_1 = CH_3 < C_6H_5 for each R_2 (secondary effect).

Kinetics. Second-Order Complex Formation Studies. The rate of complex formation was studied directly for the aceto-, benzo-, and *N*-phenylbenzohydroxamic acid systems. Complex formation rate constants were obtained for all six ligands from relaxation experiments described below.

Complex formation was treated as a second-order process approaching equilibrium. Taking into consideration the hydrolysis of $Fe(H_2O)_6^{3+}$ and the hydroxamic acid dissociation equilibrium, the simplest mechanism to consider is presented in Scheme A (coordinated H_2O is omitted for clarity). The

Scheme A

$$\text{path 2}\quad FeOH^{2+} + HA \rightleftharpoons FeA^{2+} \qquad k_2/k_{-2},\ Q_f'' \tag{4}$$

$$+H^+ \Big\| -H^+ \qquad K_h \tag{5}$$

$$\text{path 1}\quad Fe^{3+} + HA \rightleftharpoons FeA^{2+} + H^+ \qquad k_1/k_{-1},\ Q_f \tag{6}$$

$$-H^+ \Big\| +H^+ \qquad K_a \tag{7}$$

$$\text{path 3}\quad Fe^{3+} + A^- \rightleftharpoons FeA^{2+} \qquad k_3/k_{-3},\ Q_f' \tag{8}$$

integrated rate equation for Scheme A (eq 9) can be derived for this mechanism assuming that the proton-transfer equilibria (eq 5 and 7) are rapid, and by imposing the experimental condition that $[HA]_{tot} = [Fe(III)]_{tot} = C_{tot}$. Complex formation kinetic data for aceto-, benzo-, and *N*-phenylbenzohydroxamic acid are adequately described by eq 9 over the extent of reaction studied (at least 5–6 half-lives), the $[H^+]$ range from 0.03 to 0.8 M, and at 0.4 and 0.8 M ionic strength. As an additional check on the validity of eq 9, k_{exp}^{form} values computed using this equation were inserted into the simple second-order rate law for nonreversible reactions and were found to correctly predict the observed initial rates for complex formation.

$$\frac{1}{d}\ln\left(\frac{2c[FeA^{2+}] + b - d}{2c[FeA^{2+}] + b + d}\right) = \frac{1}{d}\ln\left(\frac{b-d}{b+d}\right) + k_{exp}^{form}t \tag{9}$$

$$d = (b^2 - 4ac)^{1/2} \tag{10}$$

$$a = C_{tot}^2 c \tag{11}$$

$$b = -(2C_{tot}c + [H^+]/Q_f) \tag{12}$$

$$c = (1 + K_h/[H^+])^{-2} \tag{13}$$

$$k_{exp}^{form} = k_1 + (k_2K_h + k_3K_a)/[H^+] \tag{14}$$

The experimental second-order rate constants, k_{exp}^{form}, for complex formation obtained from a linear least-squares fit of the data to eq 9 are listed in Table II for aceto-, benzo-, and *N*-phenylbenzohydroxamic acid.[42] Figure 2 is a representative plot of k_{exp}^{form} vs. $[H^+]^{-1}$ according to eq 14 for the reaction of iron(III) with *N*-phenylbenzohydroxamic acid. k_1 values obtained from the intercepts of similar plots are listed in Table III. Note that the justification for assigning a nonzero intercept (i.e., $k_1 > 0$) to plots such as shown in Figure 2 is that an acid-dependent aquation path (k_{-1}) is readily apparent from aquation studies (see below). The principle of microscopic reversibility then requires a k_1 path to be operative. In addition, the results from aquation studies allow for the calculation of k_1 independently, and the calculated and experimental values compare favorably.

According to eq 14, the slope of the plot in Figure 2 may be

Table III. Kinetic Parameters Corresponding to Scheme A

$R_1C(O)$-$N(OH)R_2$ R_1	R_2	k_1, M^{-1} s^{-1} (25.0 °C)	$\Delta H^{\ddagger}_1$,[a] kcal/mol	$\Delta S^{\ddagger}_1$,[a] eu	$10^{-3}k_2$, M^{-1} s^{-1} (25.0 °C)	$\Delta H^{\ddagger}_2$,[b] kcal/mol	$\Delta S^{\ddagger}_2$,[b] eu	10^3k_{-1},[c] M^{-1} s^{-1} (25.0 °C)	$\Delta H^{\ddagger}_{-1}$,[c,d] kcal/mol	$\Delta S^{\ddagger}_{-1}$,[c,d] eu	10^3k_{-2},[c] s^{-1} (25.0 °C)	$\Delta H^{\ddagger}_{-2}$,[c,d] kcal/mol	$\Delta S^{\ddagger}_{-2}$,[c,d] eu
CH_3	H	1.2 (0.8)[f]	9.2	−24	2.0(0.3)[c,f]	4.8(0.4)[c,f]	−27(1)[c,f]	92(1) 119(1)[h]	6.9(0.3)	−40(1)	82(1) 76(0.8)[h]	17.8(0.2)	−3.5(1)
C_6H_5	H	4.4(3.8)[f]	14.5	−7	4.3(0.4)[c,f]	8.6(0.3)[c,f]	−13(1)[c,f]	34(0.5)	12.1(0.5)	−25(2)	29(0.5) 43(1)[g]	16.1(0.3) 16.4(0.2)[g]	−11(1) −10(1)[g]
CH_3	C_6H_5	2.1[e]	15.3	−6	1.3 (0.6)[c]	6.9(1.7)[c]	−21(1)[c]	9.0(0.1)	14.0 (0.6)	−21(3)	8.2(0.1)	17.9(0.2)	−8(1)
C_6H_5	C_6H_5	1(1)[f]	14.5	−9	2.3(0.1)[c,f]	7.7(0.4)[c,f]	−18(1)[c,f]	6.9(0.1)	13.5(0.3)	−24(1)	11(0.1) 15(0.1)[g]	16.0(0.1) 15.6(0.1)[g]	−14(1) −15(1)[g]
CH_3	CH_3	2.1[e]	11.9	−17	1.2[i]	7.5(0.7)[c]	−19(1)[c]	5.2(0.1)	11.3(0.2)	−31(1)	4.8(0.1)	15.6(0.2)	−17(1)
C_6H_5	CH_3	1.4[e]	16.5	−2	0.67(0.03)[c]	6.6(0.1)[c]	−23(1)[c]	2.8(0.1)	15.5(0.5)	−19(2)	2.7(0.1)	13.6(0.5)	−24(3)

[a] Activation parameters for complex formation via path 1 calculated from $\Delta H^{\ddagger}_{-1}$, $\Delta S^{\ddagger}_{-1}$, $\Delta H_f°$, and $\Delta S_f°$. [b] Measured over the following temperature ranges (R_1, R_2, T_{range}): CH_3, H, 2.5–51.3 °C; C_6H_5, H, 2.0–50.4 °C; CH_3, C_6H_5, 25.0–51.3 °C; C_6H_5, C_6H_5, 15.3–50.3 °C; CH_3, CH_3, 14.8–49.3 °C; C_6H_5, CH_3, 13.8–45.7 °C. I = 2.00 M ($NaClO_4/HClO_4$) (first two systems also at I = 0.41 M and fourth system also at 0.81 M). [c] Calculated from results of relaxation studies, k_{exp}^{rel}, listed in Tables V–XI using eq 19.[42] I = 2.00 M ($NaClO_4/HClO_4$). [d] Measured over the following temperature ranges (R_1, R_2, T_{range}): CH_3, H, 15.6–45.7 °C; C_6H_5, H, 16.5–50.8 °C; CH_3, C_6H_5, 25.0–51.3 °C; C_6H_5, C_6H_5, 14.3–54.1 °C; CH_3, CH_3, 14.8–49.3 °C; C_6H_5, CH_3, 13.8–45.7 °C. I = 2.00 M ($NaClO_4/HClO_4$). [e] Calculated from the expression $k_1 = Q_fk_{-1}$. I = 2.00 M ($NaClO_4/HClO_4$). [f] Calculated from results of studies of kinetics of formation, k_{exp}^{form}, listed in Tables II and IV using eq 14.[42] I = 0.81 M ($NaClO_4/HClO_4$). [g] Calculated from kinetic data obtained at constant $[H^+]$ (Table XI) using eq 18 and formation rate data for k_2 and activation parameters for k_{-1}.[42] I = 0.81 M ($NaClO_4/HClO_4$). [h] Each value represents a k_{-1} (k_{-2}) value determined independently from two separate sets of 20 independent determinations of k_{exp}^{rel} over the $[H^+]$ range 0.01–1.0 M for the $CH_3C(O)N(OH)H$ system. The agreement between values is a measure of the absolute reproducibility of the system. The number in brackets is a measure of the precision of a particular data set. [i] Calculated from activation parameters.

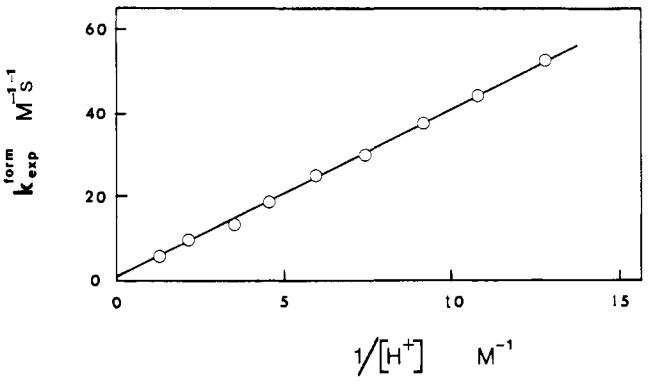

Figure 2. k_{exp}^{form} plotted as a function of $[H^+]^{-1}$ according to eq 14 for $[Fe(C_6H_5C(O)N(O)C_6H_5)(H_2O)_4]^{2+}$ complex formation at 25 °C. See Table II for data and conditions.[42]

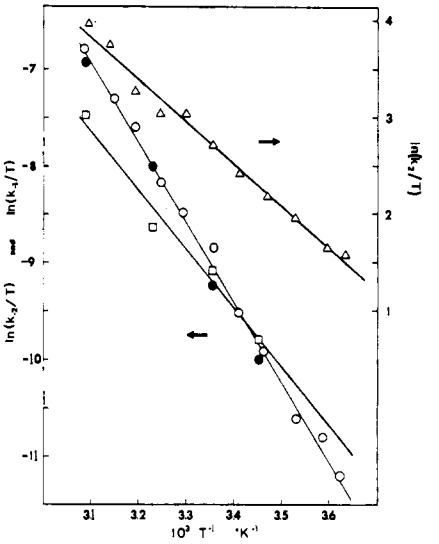

Figure 3. Temperature dependence for $[Fe(C_6H_5C(O)N(O)H)(H_2O)_4]^{2+}$ complex formation and dissociation. △ $\ln k_2/T$ vs. $1/T$. k_2 computed using data from Table IV and eq 15. □, $\ln k_{-1}/T$ vs. $1/T$. k_{-1} computed using data from Table VI and eq 19. ●, $\ln k_{-2}/T$ vs $1/T$. k_{-2} computed using data from Table VI and eq 19. ○ $\ln k_{-2}/T$ vs. $1/T$. k_{-2} computed using data from Table XI and eq 18.[42]

interpreted according to path 2 and/or path 3 of Scheme A. This ambiguity may be eliminated in the following way. For example, in the case of benzohydroxamic acid, the slope of this plot is 6.7 s^{-1}. If we assume that only path 3 is operative (i.e., $k_2K_h \sim 0$), then $k_3K_a = 6.7$ s^{-1} (eq 14). Since the acid dissociation constant, K_a, obtained at conditions identical with those of the kinetic studies is 1.3×10^{-9} M,[32] then k_3 must be 5.2×10^9 M^{-1} s^{-1}. This is much too high a value for substitution at an aqueous iron(III) center. Similar unreasonably high values were obtained for the other ligands when path 3 was assumed to be operative. Alternatively, based on the known reactivity of $Fe(H_2O)_6^{3+}$ and $Fe(H_2O)_5OH^{2+}$, reasonable values can be assumed for k_3 ($\sim 10^1$ M^{-1} s^{-1}) and k_2 ($\sim 10^3$ M^{-1} s^{-1}),[27] This approach yields $k_2K_h/k_3K_a \sim 10^8$ using 10^{-3} M for K_h[34] and 10^{-9} M for K_a.[32] Therefore path 3 can make only an insignificant contribution to the total rate of complex formation at our conditions. The k_2 values listed in Table III for aceto-, benzo-, and *N*-phenylbenzohydroxamic acid were obtained from the slope of the k_{exp}^{form} vs. $[H^+]^{-1}$ plots assuming that path 3 was not operative and using literature data for K_h.[43] During the course of our investigation a paper appeared which reported a value corresponding to k_2 for acetohydroxamic acid which is in reasonable agreement with our results for this ligand.[26]

The experimental second-order rate constants, k_{exp}^{form}, for complex formation were also determined over the temperature range from 2 to 50 °C for aceto- and benzohydroxamic acid and from 15 to 50 °C for *N*-phenylbenzohydroxamic acid. These k_{exp}^{form} values were obtained from linear least-squares fits of the data to eq 9. Data were collected at a constant $[H^+]$ such that the k_1 term in eq 14 is negligible and k_2 can be calculated from eq 15. The k_{exp}^{form} values listed in Table IV[42] were obtained in this way and were used along with literature data for K_h[43] to calculate k_2 at each temperature. Activation parameters ($\Delta H^{\ddagger}_2$ and $\Delta S^{\ddagger}_2$) were obtained from plots of $\ln(k_2/T)$ vs. $1/T$ such as shown in Figure 3 for benzohydroxamic acid, and are listed in Table III.

$$k_{exp}^{form} = k_2K_h/[H^+] \quad (15)$$

Kinetics. Relaxation Studies. Relaxation kinetic studies were carried out by rapidly increasing the $[H^+]$ of an iron(III)-hydroxamic acid complex solution (where $[Fe(III)]_{tot} = [HA]_{tot}$) from 0.01 to 0.025–1.05 M. This results in the measurement of a first-order rate constant, k_{exp}^{rel}, which corresponds to the relaxation to a new equilibrium position. Tables V–X are a compilation of first-order relaxation rate constants obtained as a function of $[H^+]$ at various temperatures from 0 to 50 °C for all six iron(III)-hydroxamic acid systems.[42] Figure 4 is a representative plot of these data at 25 °C for

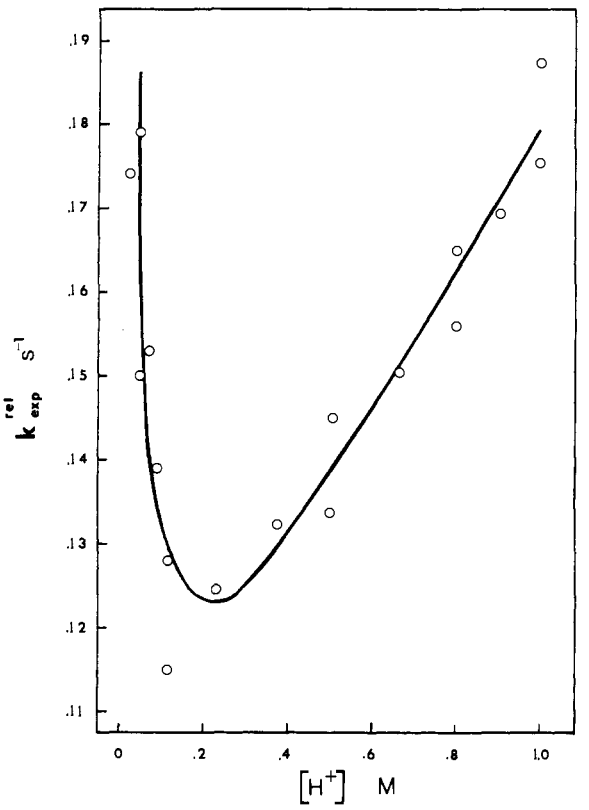

Figure 4. Plot of k_{exp}^{rel} vs. $[H^+]$ for the $[Fe(CH_3C(O)N(O)H)(H_2O)_4]^{2+}$ system at 25 °C. See Table V for data and conditions.[42] Each data point represents an average of six independent determinations of k_{exp}^{rel}; standard deviations are smaller than the data point size. The solid line represents a least-squares fit of the data to eq 16 and 18.

$[Fe(CH_3C(O)N(O)H)(H_2O)_4]^{2+}$. The solid line represents a least squares fit of the experimental data to a three-parameter equation

$$k_{exp}^{rel} = a + \frac{b}{[H^+]} + c[H^+] \quad (16)$$

A good fit of eq 16 to the relaxation rate constants was obtained for all six hydroxamic acid ligands over the temperature range investigated. A two-parameter equation which would provide a good fit to all of the data could not be found for any of the six hydroxamic acids.

When the reaction mechanism shown in Scheme A is treated as a relaxation process at the conditions where $[Fe(III)]_{tot} = [HA]_{tot} = C_{tot}$, then the equation

$$k_{exp}^{rel} = 2k_1(C_{tot} - [FeA^{2+}]_e) + k_{-2} + k_{-3} + \frac{(2k_2K_h + 2k_3K_a)(C_{tot} - [FeA^{2+}]_e)}{[H^+]} + k_{-1}[H^+] \quad (17)$$

for the relaxation rate constant, k_{exp}^{rel}, may be derived. The equilibrium complex concentration, $[FeA^{2+}]_e$, was determined from Abs_e/ϵ. Using k_1 values obtained from formation kinetic studies it can be shown that $2k_1(C_{tot} - [FeA^{2+}]_e)$ is small compared to all other terms in eq 17. Since k_3 and k_{-3} can be assumed to be zero as discussed above, eq 17 simplifies to

$$k_{exp}^{ret} = k_{-2} + \frac{2k_2K_h(C_{tot} - [FeA^{2+}]_e)}{[H^+]} + k_{-1}[H^+] \quad (18)$$

This equation is of the same form as the empirical eq 16, where $a = k_{-2}$, $b = 2k_2K_h(C_{tot} - [FeA^{2+}]_e)$, and $c = k_{-1}$.[44] Values for the rate constants k_{-1}, k_{-2}, and k_2 (Table III) were obtained from a least-squares fit of the data to eq 18 rearranged as shown in the equation

$$k_{exp}^{rel}[H^+] = 2k_2K_h(C_{tot} - [FeA^{2+}]_e) + k_{-2}[H^+] + k_{-1}[H^+]^2 \quad (19)$$

These values for k_{-1}, k_{-2}, and k_2 were then substituted into eq 18 and found to adequately fit the observed k_{exp}^{rel} values, as shown in Figure 4 for $[Fe(CH_3C(O)N(O)H)(H_2O)_4]^{2+}$.

A total of 450 k_{exp}^{ret} values (each representing an average of six determinations) were obtained for all six monohydroxamatoiron(III) complexes at various $[H^+]$ and temperatures from 0 to 50 °C (see Tables V-X).[42] Each microscopic rate constant was determined from 15 to 20 k_{exp}^{ret} values at a given temperature. Activation parameters ($\Delta H^{\ddagger}$, $\Delta S^{\ddagger}$) were obtained from relaxation experiments by plotting each of the derived rate constants (k_2, k_{-1}, and k_{-2}) as $\ln(k/T)$ vs. $1/T$. See Figure 3 for a representative plot of $\ln(k/T)$ vs. $1/T$ for $[Fe(C_6H_5C(O)N(O)H)(H_2O)_4]^{2+}$. Activation parameters for complex formation via path 1 ($\Delta H^{\ddagger}_1$, $\Delta S^{\ddagger}_1$) were calculated from the corresponding aquation parameters ($\Delta H^{\ddagger}_{-1}$, $\Delta S^{\ddagger}_{-1}$) and thermodynamic parameters ($\Delta H_f°$, $\Delta S_f°$). These activation parameters are also listed in Table III.

As a check on the activation parameters derived from the experiments described above, these parameters were redetermined for benzo- and *N*-phenylbenzohydroxamic acid using constant $[H^+]$ and variable temperature (see Table XI).[42] k_{-2} values were then computed from eq 18 by using the activation parameters determined at variable $[H^+]$ to correct k_{exp}^{rel} for the effects of the k_2 and k_{-1} terms. The activation parameters for k_{-2} determined in this manner are in very good agreement (Table III) with those determined from the $[H^+]$ and temperature-dependence studies described above. As a further test of internal consistency, microscopic rate constants, k_2, k_{-1}, and k_{-2}, computed from activation parameters were compared with the corresponding constants calculated from k_{exp}^{rel} values obtained at 25 °C. Excellent agreement was found in all cases.

Data also included in Tables II-XI show that kinetic parameters for complex formation and dissociation are not sensitive to ionic strength changes over the range from 0.4 to 2.0 M.[42]

Discussion

Equilibrium Studies. Hydroxamic acid dissociation constant values, pK_a, and the associated temperature dependencies are available at the same experimental conditions as the iron(III) complex formation constant results.[32] These pK_a values exhibit a systematic variation with the R_1 and R_2 substituents (Table I). Since stabilization of the negative charge on O_2 in the hydroxamate ion is possible only through induction, the delocalization of the lone pair of electrons on N to provide a formal positive charge adjacent to the negative charge on O_2 is of importance in determining acid strength. This delocalization may be influenced by the inductive and/or resonance effects of the carbonyl function, R_1, and R_2.[32]

Monohydroxamatoiron(III) complex thermodynamic stability follows a definite trend as the R_1 and R_2 substituents are systematically varied (Table I). However, this trend is not the same as that found for the pK_a values, since in this case R_2 shows the major influence on Q_f. Our results indicate that the driving force for complex formation (eq 1) is due to the entropy change alone (i.e., $\Delta H_f° > 0$), which is nearly constant for all six systems (17 eu ± 10%), and which clearly reflects the chelate effect. The enthalpy changes, although small, represent 13-46% of the $T\Delta S_f°$ term at 25 °C and correlate with the variations in $\ln Q_f$ (slope = −1.1 ± 0.4 kcal/mol). This result is supported by the fact that a plot of $\Delta H_f°$ vs. $\Delta S_f°$ is linear ($R = 0.91$) with an isothermal temperature of 380 (17) K, indicating that at the conditions of our experiments (2-50 °C)

the *variations* in monohydroxamatoiron(III) complex stabilities are due to variations in $\Delta H_f°$.

Path 3 in Scheme I was eliminated as an experimentally accessible path on the basis of our kinetic results (see above). However, the availability of pK_a data[32] at identical conditions with our complex formation equilibrium data allows the equilibrium quotient, Q_f', for the hypothetical reaction shown in reaction 8 to be calculated. The corresponding enthalpy ($\Delta H_f°'$) and entropy ($\Delta S_f°'$) values may also be computed from the temperature dependence of Q_f and K_a.[32] These data are listed in Table I and show that complexation of $Fe(H_2O)_6^{3+}$ by the anions of the hydroxamic acids studied is exothermic, with large positive entropy changes. This is consistent with strong chelate bond formation and charge neutralization. Unfortunately, relevant thermodynamic parameters for Fe_{aq}^{3+} chelation are not available in the literature for comparison.

The influence of R_1 and R_2 on the affinity of the hydroxamate ion for $Fe(H_2O)_6^{3+}$ relative to H^+_{aq} is illustrated in Figure 5, where the equilibrium quotient for reaction 8 (Q_f') has been plotted as a function of the equilibrium quotient for the reverse of reaction 7 (K_a^{-1}). The slope of 0.5 indicates that as the proton basicity of the hydroxamate ion increases so does its affinity for Fe_{aq}^{3+}, but that variations in R_1 and R_2 have a greater influence on $\Delta(\Delta G_a°)$ than on $\Delta(\Delta G_f°')$. The relative magnitudes of Q_f' and K_a^{-1} indicate that the hydroxamate ion has a greater affinity for Fe_{aq}^{3+} than H^+_{aq}. This is presumably due to the higher positive charge on Fe_{aq}^{3+} and the chelate effect. It is significant that the two hydroxamates which lie above the line in Figure 5 are those cases where $R_2 = CH_3$. That is, when $R_2 = CH_3$ the hydroxamate ion has a higher affinity for Fe_{aq}^{3+} than one would expect based on their pK_a values.

The results of the equilibrium studies can be interpreted on the basis of resonance forms II and III for the monohydroxamatoiron(III) complex. (Positive and negative signs represent formal charges in the hydroxamate ion.) Increasing inductive electron donor strength of R_2 should enhance the relative contribution of resonance form III and thereby increase Q_f (reaction 1). The delocalization of the N atom lone pair of electrons results in an increase in negative charge density on O_1, which would be expected to enhance the iron(III)-carbonyl oxygen bond strength (Fe-O_1).

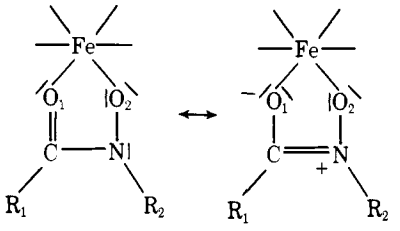

II III

The consideration of resonance forms II and III allows us to rationalize the relative ordering of the Q_f values in Table I with changes in R_2 substituents.[45] Q_f values change in regular intervals as expected from changes in σ^+ parameters for the R_2 substituents.[46] This is consistent with a contribution from resonance form III, since σ^+ parameters reflect both resonance and inductive effects on the stabilization of a positive charge delocalized in a π system.[47]

A buildup of negative charge density on O_1 when $R_2 = CH_3$ does not correspondingly enhance the hydroxamate ion's affinity for H^+ (in aqueous solution), since protonation occurs at O_2. As a result the two data points for $R_2 = CH_3$ appear above the line shown in Figure 5. Inductive R_2 stabilization of the free hydroxamate ion would have a proportional influence on both equilibria shown in eq 7 and 8.

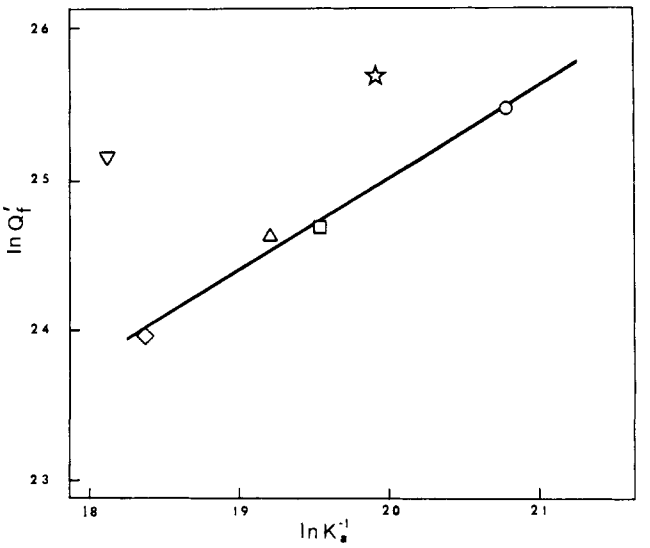

Figure 5. Plot of ln Q_f' vs. ln K_a^{-1} at 25 °C using results from Table I and defining Q_f' and K_a^{-1} as shown in eq 8 and 7. Symbols represent the six hydroxamic acid ligands investigated, $R_1C(O)N(OH)R_2$: ○, $R_1 = CH_3$, $R_2 = H$; □, $R_1 = C_6H_5$, $R_2 = H$; △, $R_1 = CH_3$, $R_2 = C_6H_5$; ◇, $R_1 = C_6H_5$, $R_2 = C_6H_5$; ☆, $R_1 = CH_3$, $R_2 = CH_3$; ▽, $R_1 = C_6H_5$, $R_2 = CH_3$.

In summary, stabilization of the positive charge density on N in *any* way increases the stability of the hydroxamate ion and therefore the acidity of the hydroxamic acid. However, variations in monohydroxamatoiron(III) complex stabilities are influenced *only* by stabilization of the formal positive charge on N through resonance form III. This form is strongly influenced by the electron donor ability of R_2 (including both resonance and inductive effects as measured by σ^+).

Kinetics and Mechanism. Reaction Scheme A shows three parallel paths to products. Path 3 was eliminated as a possibility for all six ligands on the basis of the magnitude of the forward rate constant and the ligand pK_a values. Thus the systems reported here represent one of the few cases for Fe_{aq}^{3+} substitution reactions with weak acid ligands in which an unambiguous assignment of the $[H^+]$ dependence is possible.[26,28,48-50] Our thermodynamic and kinetic data, along with published data for $Fe(H_2O)_6^{3+}$ hydrolysis, are internally consistent in that $\Delta G^{\ddagger}$ values for the aquation reaction paths obtained from direct kinetic measurements compare favorably with $\Delta G^{\ddagger}$ values computed indirectly (see Table XII). This good agreement is strong evidence which further substantiates paths 1 and 2 shown in Scheme A.

Having established the validity of a parallel path mechanism, we will now consider the details of each reaction path. Rate constants at 25 °C for the forward reaction paths (k_1 and k_2, Table III) are comparable in magnitude to literature values for uncharged monodentate ligands reacting with $Fe(H_2O)_6^{3+}$ and $Fe(H_2O)_5(OH)^{2+}$.[27] This suggests that ring closure in the reactions reported here is rapid relative to initial bond formation.

The small magnitude of k_1 and the high reactivity of $Fe(H_2O)_5OH^{2+}$ prevented the direct determination of k_1 as a function of temperature at our conditions and using our methods. Activation parameters were directly obtained, however, for k_2. The isokinetic plot shown in Figure 6A demonstrates that all six ligands studied react via a common mechanism in path 2.[48] Inclusion of activation parameters for water exchange on $Fe(H_2O)_5OH^{2+}$ in Figure 6A suggest that the net activation processes in water exchange are similar to those involved during complexation of $Fe(H_2O)_5OH^{2+}$ by the monohydroxamic acids studied.[51,53]

Table XII. Comparison of Calculated and Observed $\Delta G^{\ddagger}$ Values

$R_1C(O)N(OH)R_2$		$\Delta G^{\ddagger}_{-1}$[a] (exptl), kcal/mol	$\Delta G^{\ddagger}_{-1}$[b] (calcd), kcal/mol	$\Delta G^{\ddagger}_{-2}$[a] (exptl), kcal/mol	$\Delta G^{\ddagger}_{-2}$[c] (calcd), kcal/mol
R_1	R_2				
CH_3	H	18.7	20.1	18.9	19.6
C_6H_5	H	19.5	19.6	19.6	19.3
CH_3	C_6H_5	20.2		20.3	20.2
C_6H_5	C_6H_5	20.4	20.7	19.9	19.9
CH_3	CH_3	20.6		20.6	20.3
C_6H_5	CH_3	21.0		21.0	20.3

[a] Computed from rate constants obtained at 25.0 °C. [b] Computed from $\Delta G^{\ddagger}_{-1} + \Delta G_f^{\circ} = \Delta G^{\ddagger}_1$. [c] Computed from $\Delta G^{\ddagger}_{-2} + \Delta G_f^{\circ} = \Delta G_h^{\circ} + \Delta G^{\ddagger}_2$, where ΔG_h° was obtained from the literature.[43]

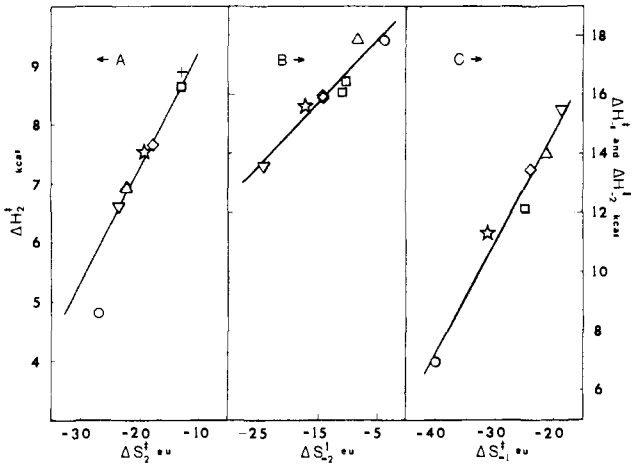

Figure 6. Isokinetic plots. Data taken from Table III. Symbols represent the six hydroxamic acid ligands investigated and are defined in the legend for Figure 5. A: k_2, + represents the activation parameters for water exchange on $Fe(H_2O)_5OH^{2+}$ obtained from ref 53. T_{iso} = 194 (12) K (neglecting data points for H_2O exchange and $CH_3C(O)N(OH)H$). B: k_{-2}, T_{iso} = 211 (25) K. C: k_{-1}, T_{iso} = 374 (35) K.

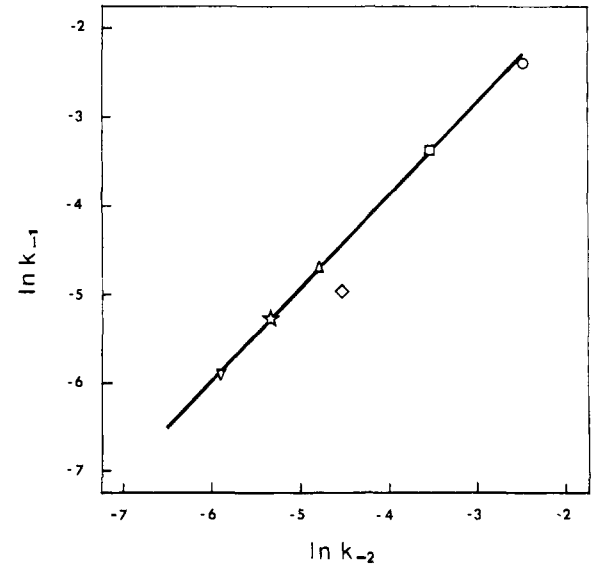

Figure 8. Plot of ln k_{-1} vs. ln k_{-2} for the monohydroxamatoiron(III) aquation reactions at 25 °C. Symbols represent the six monohydroxamatoiron(III) complexes investigated and are defined in the legend for Figure 5. Slope = 1.04 (0.09).

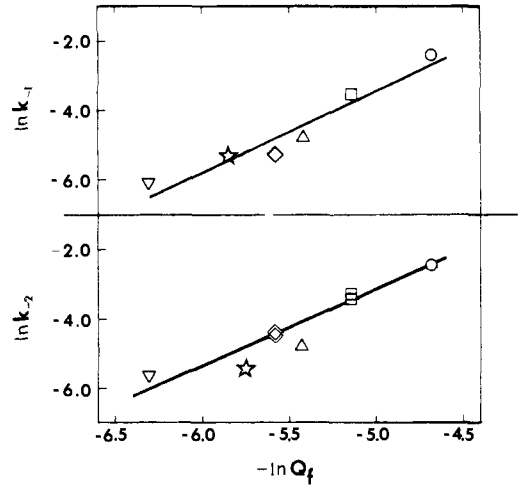

Figure 7. Plots of ln k_{-1} and ln k_{-2} vs. $-\ln Q_f$ for the monohydroxamatoiron(III) aquation reactions at 25 °C. Rate constants computed using activation parameters from Table III; Q_f values obtained from Table I. Symbols represent the six monohydroxamatoiron(III) complexes investigated and are defined in the legend for Figure 5. Slopes for the upper and lower plots are 2.4 (0.4) and 2.2 (0.3), respectively.

Figure 7 is a plot of ln k_{-1} and ln k_{-2} as a function of $-\ln Q_f$. The linearity of these plots shows that the variations in Q_f with the substituents R_1 and R_2 parallel the corresponding variations in the aquation rate constants k_{-1} and k_{-2}. In both cases these plots exhibit a slope of ca. 2. If one makes the reasonable assumption that all of these systems in dissociated form (i.e., $Fe(H_2O)_6^{3+}$ and HA) have approximately the same energy, then, based on typical reaction coordinate diagram arguments, this LFER may be interpreted to mean that a specific pair of R_1 and R_2 substituents will produce a stabilizing effect on the ground-state energy of the monohydroxamatoiron(III) complex and a destabilizing effect on the transition state.

Figure 8 shows that there is a linear relationship between ln k_{-1} and ln k_{-2} with unit slope. The theoretical basis for relating these quantities has been discussed elsewhere[54] and is usually interpreted to mean that both paths exhibit similar mechanisms. However, the magnitudes and variations in the activation parameters for both processes are widely different. This is best illustrated using isokinetic plots (Figures 6B and 6C). The linearity exhibited by these plots suggests that all six monohydroxamatoiron(III) complexes undergo aquation via the same mechanism.[48] However, the widely different isokinetic temperatures for aquation via paths 1 and 2 show that at 25 °C variations in k_{-1} are controlled by changes in $\Delta H^{\ddagger}_{-1}$ and variations in k_{-2} are controlled by changes in $\Delta S^{\ddagger}_{-2}$. The $\Delta H^{\ddagger}$ and $\Delta S^{\ddagger}$ ranges for aquation via paths 1 and 2 also differ significantly. Consistent with transition-state theory, the isothermal temperature, 380 (17) K, compares very well with the isokinetic temperature for aquation via path 1, 374 (35) K. These activation parameters form the basis for the following discussion of the details of the stepwise processes which make up paths 1 and 2.

Scheme B[56]

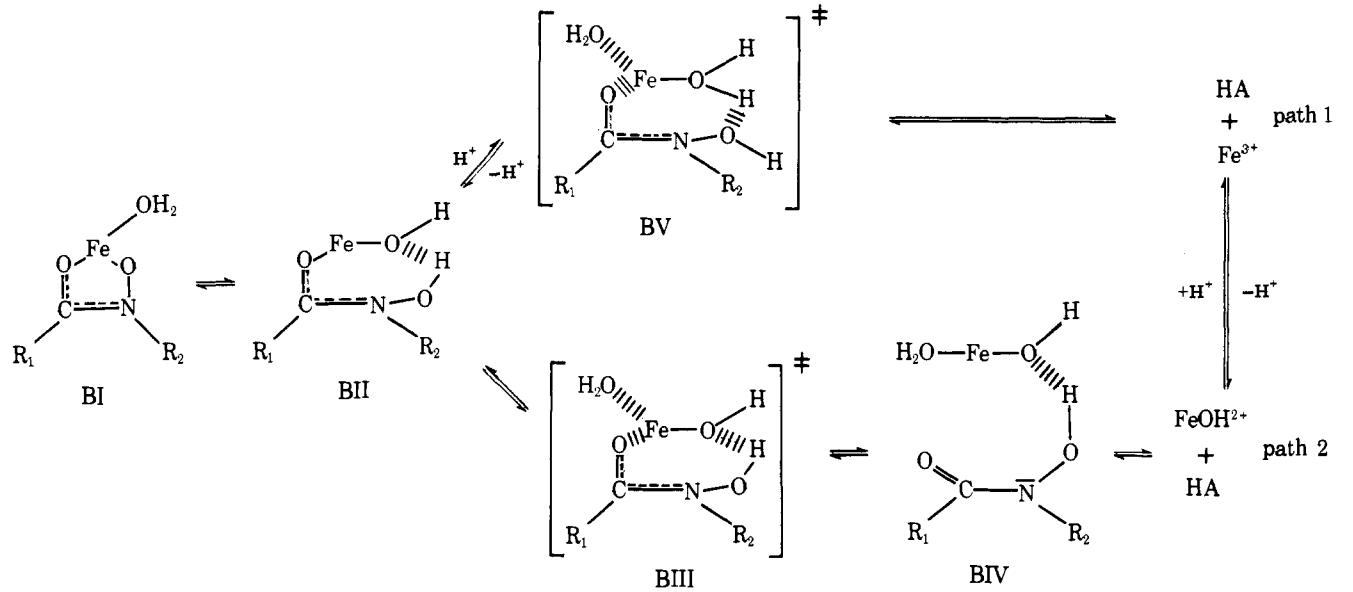

At 25 °C the $\Delta H^{\ddagger}_{-2}$ makes the major contribution to the free energy of activation for the acid-independent aquation path. However, the variations in ln k_{-2} with substituents R_1 and R_2 show a positive correlation with variations in $\Delta S^{\ddagger}_{-2}$. For constant $\Delta H^{\ddagger}_{-2}$ values, transition-state theory predicts that $\Delta S^{\ddagger}_{-2}$ will be linearly related to ln k_{-2} with slope = R. This is borne out using values for $\Delta S^{\ddagger}_{-2}$ and ln k_{-2} (from Table III) for which $\Delta H^{\ddagger}_{-2}$ is constant. The results are consistent for all six systems in that the ions which deviate from the line in a plot of ln k_{-2} vs. $\Delta S^{\ddagger}_{-2}$ do so in the manner predicted based on their $\Delta H^{\ddagger}_{-2}$ values. Therefore, the observed variations in k_{-2} are due to variations in $\Delta S^{\ddagger}_{-2}$ (with a small additional but not totally constant contribution from $\Delta H^{\ddagger}_{-2}$). Since ln k_{-2} and ln Q_f form a LFER, the variations in $\Delta S^{\ddagger}_{-2}$ show the same dependence on the substituents R_1 and R_2 as does Q_f.[55] This observation, coupled with the correlation between Q_f and $\Delta H_f°$, shows again that the same variations in R_1 and R_2 influence the energy of both the ground state ($\Delta H_f°$) *and* the transition state ($\Delta S^{\ddagger}_{-2}$). The variations in monohydroxamatoiron(III) complex bond enthalpy ($\Delta H_f°$) have been discussed above in terms of ability of R_1 and R_2 to affect the extent of delocalization of the lone pair of electrons on the N atom (see resonance forms II and III). This same electron pair delocalization argument may be used to rationalize the variations in $\Delta S^{\ddagger}_{-2}$, since the rigidity of the ligand should increase with increasing C-N double bond character.[45] As was observed in the equilibrium (Q_f) results, the kinetic parameters (ln k_{-2}, $\Delta S^{\ddagger}_{-2}$) correlate well with the σ^+ parameter for R_2.[46] *Thus the delocalization of the N atom lone pair of electrons into the carbonyl functionality is important in stabilizing the complex both kinetically and thermodynamically.* The results shown in Figure 5 where the ligands with $R_2 = CH_3$ lie above the line are then also rationalized in terms of the influence of the electron-donating CH_3 group on $\Delta S^{\ddagger}_{-2}$, and hence the kinetics of aquation.[55]

Reaction Scheme B represents the intermediates and transition state which may occur along the reaction coordinate for path 2. Structure BII represents the half-bonded form, which during complex formation undergoes rapid ring closure to form BI. The cyclic structure shown in BII and the transition-state structure corresponding to the rate-determining process, BIII, are consistent with the negative values for $\Delta S^{\ddagger}_{-2}$. Variations in the rigidity of this seven-membered ring, and hence the variations in $\Delta S^{\ddagger}_{-2}$, with changes in R_1 and R_2 may be caused by varying degrees of delocalization of the lone pair of electrons on N into the carbonyl functionality as noted above. As a consequence of our consideration of the mechanism for the acid-independent aquation reaction, initial bond formation in the complexation reaction is required to occur at the carbonyl oxygen (O_1).

Our activation and rate parameters for the forward and reverse reaction allow us to tentatively conclude that the primary substitution process at $Fe(H_2O)_5OH^{2+}$ may be associative, rather than dissociative, in character. The strongest point in this regard is that the energy of the transition state for aquation in path 2 is variable and follows a systematic trend with variations in the R_1 and R_2 substituents. This conclusion is based on Figure 7 where a plot of ln k_{-2} vs. $-\ln Q_f$ exhibits a slope of ca. 2, which suggests that the hydroxamic acid plays some role in determining the transition state free energy (see above). This assignment is strongly supported by the fact that the factors which cause the variations in the ground-state energies of these complexes and the variations in the energies of the transition states are very different (i.e., $\Delta H_f°$ and $\Delta S^{\ddagger}_{-2}$). Additional support for associative character in complex formation via reaction with $Fe(H_2O)_5OH^{2+}$ is the relatively large negative values for $\Delta S^{\ddagger}_{2}$.[52]

This associative character could arise as a result of one or both of the following: partial Fe-O_1 bond formation in the transition state (BIII) (i.e., an I_a process[57]), or from a H-bonding interaction which might occur in a preequilibrium step (BIV) and/or transition state (BIII).[28,58] The existence of a species such as BIV is not expected to produce a correlation between ligand pK_a and k_2 or the associated activation parameters, owing to the following compensating effects. The formation of BIV should increase k_2 by increasing the concentration of the encounter complex. However, this may be offset by the H-bonding interaction in BIV which would mediate the labilizing influence of the coordinated OH^- on the H_2O leaving group. These compensating effects may be a contributing factor to the observed small variation in k_2 values with entering ligand.

Comparison of k_2 data with data for water exchange on $Fe(H_2O)_5OH^{2+}$ also suggests, but does not prove, that there may be some associative character for path 2. If one assumes a value of 0.3 M^{-1} [59] for an outer-sphere association constant for $Fe(H_2O)_5OH^{2+}$ and $R_1C(O)N(OH)R_2$, and a solvation number of 10 for $Fe(H_2O)_5OH^{2+}$, then one can correct our experimental k_2 values by the ratio 10/0.3 in order to calculate a first-order water exchange rate constant at 25 °C. First-order water exchange rate constants calculated in this way range from 20 to 140 × 10^3 s^{-1}, which exceeds the published values

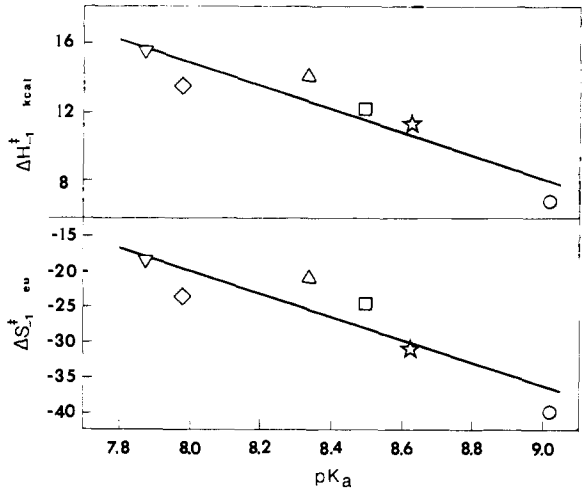

Figure 9. Plot of activation parameters ($\Delta H^{\ddagger}_{-1}$ and $\Delta S^{\ddagger}_{-1}$) for the monohydroxamatoiron(III) complex acid dependent aquation path (path 1) vs. hydroxamic acid pK_a values at 25 °C. Symbols represent the six monohydroxamatoiron(III) complexes investigated and are defined in the legend for Figure 5.

of 10–20 × 10^3 s^{-1} for water exchange on $Fe(H_2O)_5OH^{2+}$ at 25 °C and therefore suggests some associative character for path 2.[27,53]

The results discussed above seem to suggest that there is an associative character to complexation of $Fe(H_2O)_5OH^{2+}$ by the hydroxamic acids studied. This tentative conclusion is based in some cases on small variations in parameters. However, these conclusions appear to be valid since trends are reproducible and were observed in several parameters obtained from both the forward and reverse reactions when R_1 and R_2 were varied. The inclusion of the activation parameters from the literature[51,53] for H_2O exchange in the isokinetic plot shown in Figure 6A suggests the possibility that water exchange on $Fe(H_2O)_5OH^{2+}$ is associative also. Other workers have observed small variations in complexation rates on $Fe(H_2O)_5OH^{2+}$ and have intepreted these results more often in terms of an I_d mechanism[48] than an I_a mechanism.[49] It may be that an analysis of the corresponding aquation reactions for these other systems will suggest an associative character in some cases. The number of studies involving both complexation and aquation kinetics for a series of related ligands reacting with $Fe(H_2O)_5OH^{2+}$ is very limited,[28] preventing comparisons from being made. Furthermore, the small degree of associative character observed in the present study for path 2 may be due to a H-bonding interaction in the transition state rather than partial Fe-O_t bond formation. In that case the strict criteria for an I_a label have not been met and the associative character is more a result of a combination of ligands (OH^- and HA) than metal center and donor atom.

As indicated above, the variations in the rate of the acid-dependent aquation reaction (path 1) are $\Delta H^{\ddagger}$ controlled and the corresponding activation parameters correlate differently than those for the acid-independent path. The $\Delta S^{\ddagger}_{-t}$ values are large and negative, and make a contribution to ln k_{-1} at 25 °C which is comparable to that contribution from $\Delta H^{\ddagger}_{-t}$. Variations in R_t and R_2 produce parallel trends in ln Q_f and ln k_{-t}. As with path 2, both $\Delta S^{\ddagger}_{-t}$ and $\Delta H^{\ddagger}_{-1}$ correlate with ln k_{-t} at 25 °C in a predictable manner according to transition-state theory. Both $\Delta H^{\ddagger}_{-1}$ and $\Delta S^{\ddagger}_{-1}$ exhibit a good linear correlation with hydroxamic acid pK_a values (Figure 9). An increase in ligand basicity results in a decrease in $\Delta H^{\ddagger}_{-1}$ and $\Delta S^{\ddagger}_{-1}$.

Reaction Scheme B also includes a representation of the intermediates, and the transition state for the rate-determining step, which may occur along the reaction coordinate for path 1. In this case all of the available data can be rationalized using a simple alteration of the mechanism for path 2 where the half-bonded intermediate (BII) is allowed to undergo protonation. This step is expected to be fast relative to Fe-O_1 bond breakage and could occur at either of the two available sites, O_2 or N. Protonation of the hydroxamate ligand would cause the Fe-O_t bond to weaken due to a concomitant shift in electron density away from O_1 toward N. Since O_2 is not directly bonded to the Fe(III) center in BII, the ligand would be expected to behave similarly to the free anion and hence would explain the good correlation between $\Delta H^{\ddagger}_{-t}$ and $\Delta S^{\ddagger}_{-1}$ with pK_a. Of prime importance in this reaction scheme is the site of protonation, which may be deduced from further analysis of the variations in the activation parameters. Based on the results of the acid-independent aquation reaction (path 2), one would expect the enthalpy of activation for Fe-O_1 bond cleavage to show relatively small changes with R_1 and R_2. However, for the acid-dependent aquation reaction the enthalpy change due to protonation of the hydroxamate ligand must also be considered. This bond formation contribution should lower the enthalpy of activation relative to the acid-independent path. This is consistent with our results in that $\Delta H^{\ddagger}_{-1} \leq H^{\ddagger}_{-2}$ and $\Delta H^{\ddagger}_{-t}$ decreases with increasing ligand basicity (Figure 9). Protonation at the N atom would eliminate the resonance delocalization of the lone pair of electrons (resonance form III). This would remove electron density from O_t and weaken the corresponding bond to iron(III). This would manifest itself in a decrease in $\Delta H^{\ddagger}_{-t}$ (relative to the acid-independent path) by a constant factor, thus preventing $\Delta H^{\ddagger}_{-1}$ and $\Delta H^{\ddagger}_{-2}$ from becoming equal in magnitude for the more acidic ligands. This is contrary to our results. Therefore, on the basis of this discussion, protonation must occur at O_2. In addition, the correlation of $\Delta H^{\ddagger}_{-t}$ with ligand pK_a suggests protonation at O_2 rather than at N since pK_a values are a measure of the affinity of the O_2 site for a proton.[60] Finally, the more negative values for $\Delta S^{\ddagger}_{-1}$ (relative to $\Delta S^{\ddagger}_{-2}$) may arise as a result of bringing together a 1+ and a 2+ species in forming the transition state (BV).

As was the case in path 2, a consideration of the aquation reaction for path 1 requires initial bond formation in the complexation reaction to occur between iron(III) and O_1. In addition, it follows from the proposed mechanism that species BII represents an intermediate which may undergo dissociation by either path depending upon pH and ligand basicity.

As with path 2, the LFER between ln k_{-1} and $-\ln Q_f$ with a slope ca. 2 suggests that there may be some associative character for complexation via path 1. This mode of activation for substitution reactions at $Fe(H_2O)_6^{3+}$ has been suggested for other ligands.[48,49,52]

Although we were unable to obtain the activation parameters for k_1 directly, they can be computed from our measured k_{-t} and Q_f values (see Table III). The results of these calculations reveal a good isokinetic relationship between $\Delta H^{\ddagger}_1$ and $\Delta S^{\ddagger}_1$ (R = 0.9999) with an isokinetic temperature of 328 (18) K, which is consistent with the corresponding temperatures for k_{-t} and Q_f. The $\Delta H^{\ddagger}_t$ values computed in this way are larger than the corresponding $\Delta H^{\ddagger}_2$ values, which is consistent with weaker Fe-OH_2 bond strengths in $Fe(H_2O)_5OH^{2+}$ than in $Fe(H_2O)_6^{3+}$. The fact that activation entropy changes for complex formation via both paths ($\Delta S^{\ddagger}_1$ and $\Delta S^{\ddagger}_2$) are similar is not unexpected in view of the mechanism in Scheme B, where both steps correspond to similar processes. It is significant that variations in $\Delta H^{\ddagger}$ and $\Delta S^{\ddagger}$ with entering ligand are similar for complex formation via paths 1 and 2. Since there is an increasing acceptance that $Fe(H_2O)_6^{3+}$ reacts via an associative (I_a) mechanism,[48,49,52] this similarity makes the associative assignment to the mechanism for complexation involving $Fe(H_2O)_5OH^{2+}$ all the more reasonable.

Plots of $\Delta S^{\ddagger}_t$ and $\Delta H^{\ddagger}_1$ vs. pK_a are linear (R = 0.999 97

and 0.9997, respectively) and appear nearly identical with the corresponding plots for aquation via path 1 (Figure 9). The direct correlation between ligand basicity and activation parameters for k_1 can also be rationalized in terms of Scheme B if the reasonable assumption is made that the variations in basicity of O_2 in the neutral ligand parallel the variations in basicity of O_2 in the hydroxamate ion. The observed trends in $\Delta H^{\ddagger}_1$ can then be rationalized in terms of species BV in which the strength of the H bond in the seven-membered ring would be dependent upon the basicity of protonated O_2. This same argument explains the variations in $\Delta S^{\ddagger}_1$ in that the rigidity of the seven-membered ring would be expected to parallel the basicity of the ligand.

The observed correlation between $\Delta H^{\ddagger}_1$, $\Delta S^{\ddagger}_1$, and pK_a may also be used to ascertain the extent of O_2–H bond cleavage in the transition state, BV. Since complex formation occurs fastest for the more basic ligands, this suggests that O_2–H bond cleavage is not important in the rate-determining step. Since bond cleavage cannot occur before the rate-determining step in complex formation (i.e., path 1 does not show a dependence on $[H^+]$), this indicates that the O_2–H proton is ionized after the rate-determining step. Our proposed mechanism is consistent with this result and further suggests the presence of another intermediate (besides BII) which would lie between species BII and BV in Scheme B. This analysis is supported by Figure 8, where such a linear relationship between rate constants corresponding to different paths is expected for cases where the intermediates involved differ only by a proton.[54]

At the more basic conditions found in biological systems (e.g., pH 8 for seawater) an appreciable amount of hydroxamate anion would be present, making complexation of iron by the anion a significant reaction. Although it may be premature to apply our results to the siderophores, it is of interest to note that for the hydroxamic acids reported here complexation by the anion is greatest (largest Q_f') for the case where $R_1 = R_2$ = alkyl (methyl) (see Table I). This may be compared with the evolution of the hydroxamate siderophores of the ferrioxamine class where the hydroxamate functional groups are linked together by alkyl groups at positions corresponding to R_1 and R_2.

Acknowledgments. Financial support from NIEHS through a grant to the Duke University Marine Laboratory Marine Biomedical Center, and a Biomedical Research Support Grant, is gratefully acknowledged. B.M. acknowledges receipt of an ACS, North Carolina Section, Centennial Scholarship Award and a Graduate School Award.

Supplementary Material Available: Rate constant data, Tables II and IV–XI (15 pages). Ordering information is given on any current masthead page.

References and Notes

(1) For a recent review of the organic chemistry of hydroxamic acids see: Bauer, L.; Exner, O. *Angew. Chem.* **1974**, *13*, 376.
(2) For a recent review see: Chatterjee, B. *Coord. Chem. Rev.* **1978**, *26*, 281.
(3) See for example: (a) Brandt, W. W. *Rec. Chem. Prog.* **1960**, *21*, 159, and references cited therein. (b) Mojumdar, A. K., *Int. Ser. Monogr. Anal. Chem.* **1972**, *50*.
(4) Neilands, J. B. In "Inorganic Biochemistry", Eichhorn, G., Ed.; American Elsevier: New York, 1973; Chapter 5.
(5) Neilands, J. B., Ed. "Microbial Iron Metabolism", Academic Press: New York, 1974.
(6) Emery, T. In "Metal tons in Biotogical Systems", Sigel, H., Ed.; Marcel Dekker: New York, 1978; Chapter 3.
(7) Neilands, J. B. *Adv. Chem. Ser.* **1977**, *No. 162*, 3.
(8) Raymond, K. N. *Adv. Chem. Ser.* **1977**, *No. 162*, 33.
(9) Anderson, W. F., Hiller, M. C., Ed. "Development of Iron Chelators for Clinical Use", Department of Health, Education, and Welfare Publication, U.S. Government Printing Office: Washington, D.C., 1977; No. (NIH) 76-994.
(10) Zaino, E. C., Roberts, R. H., Ed. "Chelation Therapy in Chronic Iron Overload", Stratton Intercontinental Medical Book Corp.: New York, 1977.
(11) *Chem. Eng. News* **1977**, *55*(18), 24.
(12) Pitt, C. G.; Gupta, G.; Estes, W. E.; Rosenkrantz, H.; Metterville, J. J.; Crumbliss, A. L.; Palmer, R. A.; Nordquest, K. W.; Sprinkle Hardy, K. A.; Whitcomb, D. R.; Byers, B. R.; Arcenaux, J. E. L.; Gaines, C. G.; Sciortino, C. V. *J. Pharmacol. Exp. Ther.* **1979**, *208*, 12.
(13) Grady, R. W.; Graziano, J. H.; White, G. P.; Jacobs, A; Cerami, A. *J. Pharmacol. Exp. Ther.* **1978**, *205*, 757.
(14) Brown, D. A.; Chidambarama, M. V.; Clarke, J. J.; McAleese, D. M. *Bioinorg. Chem.* **1978**, *9*, 255.
(15) Lindner, Von H.; Göttlicher, S. *Acta Crystallogr., Sect. B* **1969**, *25*, 832.
(16) Zalkin, A.; Forrester, J. C.; Templeton, D. H. *J. Am. Chem. Soc.* **1966**, *88*, 1810.
(17) van der Helm, D.; Doling, M. *J. Am. Chem. Soc.* **1976**, *98*, 82.
(18) Hough, E.; Rogers, D. *Biochem. Biophys. Res. Commun.* **1974**, *57*, 73.
(19) Norrestam, R.; Stenskind, B.; Branden, C-I. *J. Mol. Biol.* **1975**, *99*, 501.
(20) (a) Sillén, L. G.; Martell, A. E. "Stability Constants of Metal-Ion Complexes", *Chem. Soc., Spec. Publ.* **1964**, *No. 17*. (b) *Ibid. Suppl. 1* **1971**, *No. 25*. (c) Martell, A. E.; Smith, R. M."Critical Stability Constants", Vol. 3; Plenum Press: New York, 1977.
(21) Schwarzenbach, G.; Schwarzenbach, K. *Helv. Chim. Acta* **1963**, *46*, 1390.
(22) Asknes, G. *Acta Chem. Scand.* **1957**, *11*, 710.
(23) Schwarzenbach, G.; Anderegg, G.; 'Eplatteniger, F. L. *Helv. Chim. Acta* **1963**, *46*, 1409, 1400.
(24) Carrano, C. J.; Raymond, K. N. *J. Chem. Soc., Chem. Commun.* **1978**, 501; *J. Am. Chem. Soc.* **1978**, *100*, 5371.
(25) Lentz, D. J.; Henderson, G. H.; Eyring, E. M. *Mol. Pharmacol.* **1973**, *6*, 514.
(26) Kujundzic, N.; Pribanic, M. *J. Inorg. Nucl. Chem.* **1978**, *40*, 729.
(27) Margerum, D. W.; Cayley, G. R.; Weatherburn, D. C.; Pagenkopf, G. K. In "Coordination Chemistry", Martell, A. E., Ed.; American Chemical Society: Washington, D.C., 1978; Vol. 2, p 1.
(28) Nakamura, K.; Tsuchida, T.; Yamagishi, A.; Fujimoto, M. *Bull. Chem. Soc. Jpn.* **1973**, *46*, 456. Cavasino, F. P.; Di Dio, E. *J. Chem. Soc. A* **1970**, 1151.
(29) A preliminary report of these results has been made: Crumbliss, A. L.; Monzyk, B. "Abstracts of Papers", 176th National Meeting of the American Chemical Society, Miami Beach, Fla., Sept 1978; American Chemical Soclety: Washington, D.C., 1978; INOR 143.
(30) Coleman, G. H.; McCloskey, C. M.; Stuart, F. A. "Organic Syntheses", Collect. Vol. III; Wiley: New York, 1955; p 668. Berndt, D. C.; Fuller, R. L. *J. Org. Chem.* **1966**, *31*, 3312. Berndt, D. C.; Sharp, J. K. *Ibid.* **1973**, *38*, 396.
(31) Gupta, V. K.; Tandon, S. G. *J. Indian Chem. Soc.* **1969**, *46*, 831.
(32) Monzyk, B.; Crumbliss, A. L., manuscript in preparation.
(33) Siddall III, T. H.; Vosburgh, W. C. *J. Am. Chem. Soc.* **1951**, *73*, 4270.
(34) Milburn, R. M. *J. Am. Chem. Soc.* **1957**, *79*, 537.
(35) Wendt, H. *Z. Elektrochem.* **1962**, *66*, 235.
(36) Sommer, B. A.; Margerum, D. W. *Inorg. Chem.* **1970**, *9*, 2517.
(37) [Fe(III)] represents the total uncomplexed iron(III) concentration, i.e., $[Fe(III)] = [Fe(H_2O)_6^{3+}] + [Fe(H_2O)_5OH^{2+}]$.
(38) Skoog, D. A.; West, D. M. "Fundamentals of Analytical Chemistry", 2nd ed.; Holt, Rinehard and Winston: New York, 1963; p 437.
(39) Coleman, J. S.; Varga, L. P.; Mastin, S. H. *Inorg. Chem.* **1970**, *9*, 1015.
(40) Job, P. *C. R. Hebd. Seances Acad. Sci.* **1925**, *180*, 938; Vosburgh, W. C.; Cooper, G. R. *J. Am. Chem. Soc.*, **1941**, *63*, 437.
(41) Although plots of eq 3 showed that the data were of very good precision ($R \geq 0.999$), values for ϵ were not determined from the intercepts of these plots as they are inherently of low precision. Rose, N. J.; Drago, R. S. *J. Am. Chem. Soc.* **1959**, *81*, 6138.
(42) See paragraph at end of paper regarding supplementary material.
(43) The data of Milburn[34] at $I = 1.0$ M ($NaClO_4$) were used to compute $\Delta H_h^\circ = 10.16$ kcal/mol and $\Delta S_h^\circ = 21.35$ eu. These values were used to compute K_h at the temperatures used in this study.
(44) Additional support for the validity of eq 18 was obtained by observing that at constant and low $[H^+]$ k_{exp}^{rel} varies linearly with $(C_{tot} - [FeA]_e)$.
(45) The trends observed with changes in R_1 and R_2 preclude a rationalization of these variations based on solvation or steric effects.
(46) σ^+ values for R_2 substituents are as follows (ref 47): H, 0.00; C_6H_5, −0.179; CH_3, −0.311.
(47) Leffler, J. E.; Grunwald, E. "Rates and Equilibria of Organic Reactions", Wiley: New York, 1963; p 203.
(48) Wilkins, R. G. "The Study of Kinetics and Mechanism of Reactions of Transition Metal Complexes", Allyn and Bacon: Boston, 1974.
(49) Gomwalk, U. D.; Lappin, A. G.; McCann, J. P.; McAuley, A. *Inorg. Chim. Acta* **1977**, *24*, 39.
(50) Fay, D. P.; Nichols, A. R.; Sutin, N. *Inorg. Chem.* **1971**, *10*, 2096.
(51) This comparison should be made with some caution, however, since activation parameters for water exchange were obtained from first-order rate constants, while the complex formation rate constants are second order.[52]
(52) Swaddle, T. W. *Coord. Chem. Rev.* **1974**, *14*, 217.
(53) Genser, E. E. 1962, AEC Report UCRL-9846.
(54) Asher, L. E.; Deutsch, E. *Inorg. Chem.* **1973**, *12*, 1774.
(55) This is true in full detail including a plot corresponding to Figure 5 where $\Delta S^{\ddagger}_{-2}$ is plotted as a function of $\ln K_a^{-1}$. This plot shows the same pattern as Figure 5, with the points corresponding to $R_2 = CH_3$ appearing below the line at more negative $\Delta S^{\ddagger}_{-2}$ values.
(56) Charges on the complexes and nonreacting coordinated H_2O have been omitted for clarity.
(57) Langford, C. H.; Gray, H. B. "Ligand Substitution Processes", W. A. Benjamin: New York, 1965.
(58) Funahashi, S.; Adachi, S.; Tanaka, M. *Bull. Chem. Soc. Jpn.* **1973**, *46*, 479.
(59) Kustin, K.; Swinehart, J. *Prog. Inorg. Chem.* **1970**, *13*, 135.
(60) Protonation at N may also be considered to be unlikely on the grounds that benzamide is only half-protonated in 34% sulfuric acid; Arnett, E. M. *Prog. Phys. Org. Chem.* **1963**, *1*, 223.